JOURNAL OF APPLIED ELECTROCHEMISTRY 23 (1993) 589–596

Analysis of irreversible oxidation wave of adsorbed CO at Pt(1 1 1), Pt(1 0 0) and Pt(1 1 0) electrodes*

H. KITA‡, H. NARUMI, S. YE, H. NAOHARA

Department of Chemistry, Faculty of Science, Hokkaido University, Sapporo, 060, Japan

Received 9 July 1992; revised 8 October 1992

The oxidation wave of CO preadsorbed at 50 mV on Pt(1 1 1), (1 0 0) and (1 1 0) electrodes in phosphate buffer solution of pH 3 was observed as a function of the sweep rate. The sweep rate dependence of the peak current and peak potential, as well as the form of the wave, were examined on the basis of the Gilman mechanism that the electron transfer from a complex consisting of CO and oxygen containing species is the rate-determining step. An electron transfer step from CO itself was excluded. The peak current and peak potential analyses and the wave simulation gave the same value for Δf, the change in the interaction energy during the formation of the activated complex from the reactants. Δf was sweep-rate and surface-structure dependent. The nature of Δf was discussed.

Nomenclature

α	symmetry factor
ϵ	reversible work required to bring an adsorbed species from its standard state
μ	electrochemical potential
ϕ	electrode potential referred to the reversible hydrogen electrode
ϕ_p	peak potential
$\Delta\phi_{1/2}$	width at half height of the oxidation wave
(a)	adsorbed state
$f(\ddagger)$	mutual interaction energy of the activated complex in RT units
$f(R)$	mutual interaction energy of the reactants in RT units
Δf	$f(\ddagger) - f(\mathrm{R})$
i	oxidation current density, mA cm^{-2}
i_p	peak current, mA cm^{-2}
k	rate constant
Q_0	electric charge, mCcm^{-2}
v	sweep rate, m Vs^{-1}

1. Introduction

It is well known that the hydrogen wave at a platinum electrode is highly reversible so that the anodic and cathodic scans give a symmetrical cyclic wave with respect to the potential axis.

The wave itself is equivalent to the pseudo-capacitance of the electrode and the latter was discussed first for the absence of the mutual interaction among adsorbed species [1] and has since been extensively studied by Conway and his coworkers [2–5]. One of the present authors treated the repulsive interaction statistical mechanically [6, 7]. The latter treatment suggested theoretically the presence of double maxima on the hydrogen wave at (1 1 0) and (1 0 0) and triple maxima at (1 1 1) electrodes, respectively. Recently, Tokuda *et al.* developed the statistical mechanical treatment for redox couples and an activated complex confined to an electrode surface at monolayer level [8] and applied to cyclic voltammetry and faradaic impedance measurements [9]. Recently, the adsorption of CO on nobel metal electrodes is reviewed, taking into account both experimental and theoretical approaches by Beden *et al.* [10].

In the present paper, the irreversible wave of the adsorbed CO oxidation is treated, where the wave is controlled by the kinetics of the oxidation. A deconvolution of the wave in terms of the adsorption isotherm [11] is inadequate since the isotherm describes the equilibrium phenomena. The present analysis of the waves observed at Pt(1 1 1), (1 0 0) and (1 1 0) planes will give information on the oxidation mechanism, including the nature of the inter-action among surface species which form the reaction atmosphere.

2. Experimental details

Platinum single crystals were prepared by Clavilier's method [12, 13]. Platinum wire of 1 mm diameter (99.99%, Tanaka Nobel Metal Corp.) was used. Between each electrochemical measurement, the crystal was treated in a gas + oxygen flame at 1000°C for a few seconds and then transferred into pure water to quench the electrode quickly [12]. In this study, three low index planes, (1 1 1), (1 0 0) and (1 1 0), were examined.

The experiments were carried out in a cell consisting of three compartments for the test, counter and refer-

* This paper is dedicated to Professor Brian E. Conway on the occasion of his 65th birthday, and in recognition of his outstanding contribution to electrochemistry.

‡ Author to whom all correspondence should be addressed.

0021-891X

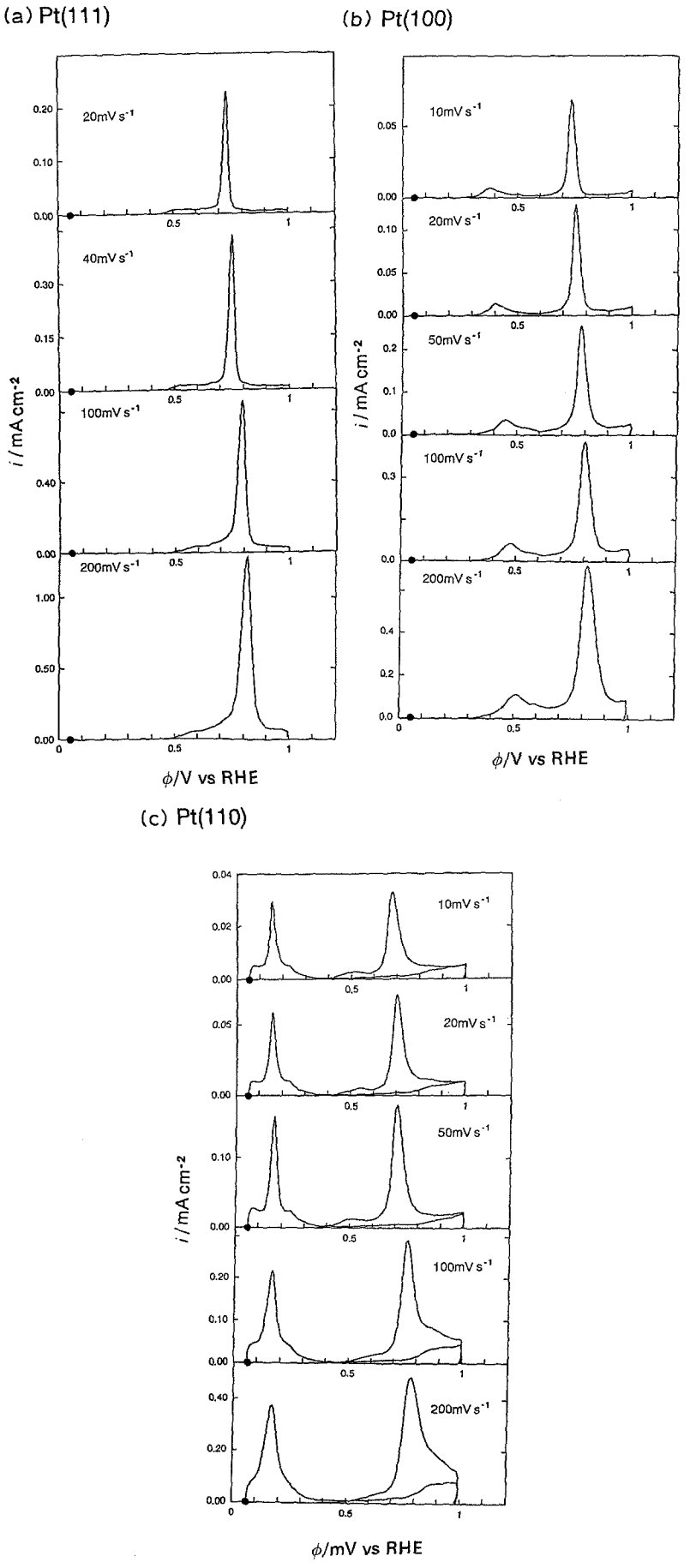

Fig. 1. Sweep dependence of the oxidation waves of CO adsorbed at 50 mV on platinum single crystal electrodes in phosphate buffer solution of pH 3. (a) Pt(1 1 1); (b) Pt(1 0 0); (c) Pt(1 1 0).

ence electrodes, each connected to gas pipe-lines of H_2, Ar and/or CO. The counter-electrode was platinized platinum of large area. The reference electrode was a reversible hydrogen electrode (RHE), to which all potentials in the text are referred.

The electrolytic solution was prepared from H_3PO_4, KH_2PO_4 (Wako Pure Chem. Co., suprapure reagent) and purified water(Milli Q system). Carbon monoxide(Seitetsu Chem. Co., 99.9% purity) and Ar(Teikoku Oxygen Co., 99.99%) were used as received in most cases. Hydrogen was purified with a commercial purifier to 99.99999% purity.

The adsorption state of CO is strongly affected by the experimental conditions. Under precise experimental conditions, an oxidation peak appears at very low potential [14, 15]. In the present study, the CO adsorbed in the hydrogen region [14] was mainly treated.

The electrode was first immersed in the solution saturated with atmospheric argon and polarized at 50 mV and kept at the same potential throughout the following adsorption procedure. Then the CO(1 atm) was bubbled for 3 min to allow CO adsorption. After the adsorption, the remaining CO was purged by bubbling argon for 15 min. The electrode was then lifted up and placed in contact with the solution through a meniscus where the solution was kept static. Argon was flowed above the solution. Special attention was given to the exclusion of traces of oxygen. A usual electrochemical setup was used for for voltammetric measurements. All data were collected at room temperature.

3. Experimental Results

Figure 1(a) to (c) show the oxidation waves of CO preadsorbed at 50 mV (denoted 50 mV CO(a)) on Pt(1 1 1), (1 0 0) and (1 1 0) electrodes in a phosphate buffer solution of pH 3 at different sweep rates. At each electrode, a large peak is observed in the double layer region, though the rear tail at Pt(1 1 0) extends into the oxygen region. In Fig. 1(c) for Pt(1 1 0), the second voltammogram was superimposed to show the overlapping in the oxygen region. The second voltammogram shows the hydrogen wave and no trace of the CO oxidation wave.

The essential nature of the peak is that it represents the 'irreversible' oxidation wave since the reverse potential sweep does not give a peak, in contrast to the hydrogen wave observed in the blank solution. In the latter case, the reverse potential sweep does give a reduction wave symmetrical with the oxidation wave.

Secondly, the oxidation wave of 50 mV CO(a) shifts in positive direction with increase in the sweep rate at the respective electrodes. This shift reflects the fact that the oxidation wave is controlled kinetically, in contrast to the case of the hydrogen wave. The hydrogen wave does not shift with sweep rate (see Fig. 1(c), hydrogen wave) and reflects directly the electrochemical adsorption isotherm of hydrogen. The isotherm represents an equilibrium phenomenon.

4. Kinetic analysis of the oxidation wave

The analysis of the wave begins with the assumption that the oxidation of CO(a) proceeds via either of two reaction schemes: In Scheme 1, the rate-determining step is the first electron transfer from CO(a), forming $CO(a)^+$ which is rapidly oxidized to CO_2 and in Scheme 2, the rate-determining step is the electron transfer from a complex consisting of CO(a) and oxygen containing species, here represented by OH(a). These are formulated as follows:

$$\text{Scheme 1:}\quad \mathrm{CO(a)} \longrightarrow \mathrm{CO(a)^+ + e^-}, \qquad \mathrm{CO(a)^+} \rightarrow\rightarrow \mathrm{CO_2} \quad (1)$$

$$\text{Scheme 2:}\quad \mathrm{[CO \cdot OH](a)} \longrightarrow \mathrm{CO_2 + H^+ + e^-} \quad (2)$$

The corresponding rate expressions are given as follows, by taking into account the interaction among surface species:

$$\text{Scheme 1:}\quad i = k\theta \exp(-\Delta f \theta) \exp\left(\frac{\alpha F v}{RT} t\right) \quad (3)$$

$$\text{Scheme 2:}\quad i = k\theta(1-\theta) \exp(-\Delta f \theta) \exp\left(\frac{\alpha F v}{RT} t\right) \quad (4)$$

where Δf represents the change in the interaction energy during the formation of the activated complex from the reactant(s);

$$\Delta f \equiv f(\ddagger) - f(\mathrm{R}), \quad (5)$$

and $(1-\theta)$ in Equation 4 represents the coverage of OH(a). Δf is a kinetic parameter which differs in nature from the interaction energy appearing in the adsorption isotherm, such as the Frumkin isotherm.

The oxidation current, on the other hand, is related to the change of θ as

$$i = -Q_0 \frac{\mathrm{d}\theta}{\mathrm{d}t} \quad (6)$$

The monolayer charge for the oxidation of CO(a), Q_0, was estimated from the peak area after the subtraction of the blank current and was taken as the charge corresponding to the full coverage ($\theta = 1$) in the following analysis. It has already been confirmed that, at this value, the electrode is completely masked from the ionization of hydrogen gas dissolved in solution at positive potentials, demonstrating the full coverage of CO(a) [16].

4.1. *Peak current, i_p, and peak potential, ϕ_p, analysis*

In the case of the reversible wave of a single electron transfer step satisfying the Frumkin isotherm with the interaction parameter, f in RT units, the peak current is given by [2–5] (see Appendix),

$$i_p = \frac{Q_0 F v}{RT(4+f)} \quad (7)$$

Equation 7 indicates that i_p is proportional to v. The peak potential, ϕ_p, is independent of v.

In the present case, i_p and ϕ_p are given as a function of the sweep rate as follows.

Scheme 1

Differentiation of Equation 3 with respect to t and the condition $di/dt = 0$ at ϕ_p gives

$$i_p = \frac{\theta_p}{1 - \Delta f \theta_p} Q_0 \frac{\alpha F}{RT} v \tag{8}$$

where θ_p is the coverage at ϕ_p.

Introduction of i_p from Equation 3 at $\phi = \phi_p$ into Equation 8 yields

$$\phi_p = a - b\left[-\frac{\Delta f \theta_p}{2.303} + \log(1 - \Delta f \theta_p) + b \log v\right] \tag{9}$$

where

$$a \equiv b \log(Q_0 \alpha F / kRT) = \text{const.}$$
$$b \equiv 2.303 RT/\alpha F = \text{const.} \tag{10}$$

Scheme 2

The same treatment was applied to Equation 4. Results are as follows:

$$i_p = \frac{\theta_p(1 - \theta_p)}{(1 - 2\theta_p) - \Delta f \theta_p(1 - \theta_p)} Q_0 \frac{\alpha F}{RT} v \tag{11}$$

$$\phi_p = a + b\left[\frac{\Delta f \theta_p}{2.303} - \log\{(1 - 2\theta_p) - \Delta f \theta_p(1 - \theta_p)\}\right] + b \log v \tag{12}$$

The above relationship between i_p, ϕ_p and v were examined by using experimental data from Fig. 1.

4.1.1. i_p against v: Figure 2 represents the plot of i_p against v. No linear relations between i_p and v hold on the respective crystal planes. Equations 8 and 11 of Schemes 1 and 2 include θ_p (Table 1). Since θ_p appears almost independent of the sweep rate, e.g., on Pt(1 0 0) 0.52, 0.57, 0.55, 0.55, 0.52 at v = 10, 20, 50, 100, 200 mV s^{-1}, the absence of a linear relationship suggests the interaction, Δf, to be sweep-rate dependent. The value of Δf may be estimated if α is known. The value of α is evaluated below.

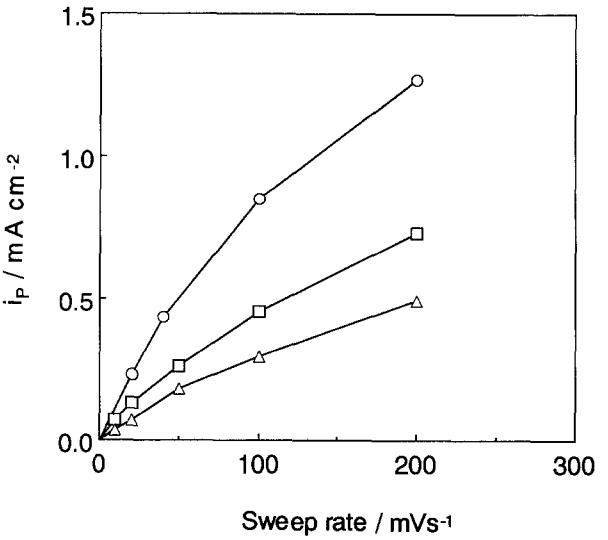

Fig. 2. Peak current against sweep rate at 50 mV CO(a) oxidation on (○) Pt(1 1 1), (□) Pt(1 0 0) and (△) Pt(1 1 0) electrodes in phosphate buffer solution of pH 3.

4.1.2. ϕ_p against log v: ϕ_p is plotted against log v on the respective planes in Fig. 3. A straight line holds in each case. The slope (b) and the corresponding α estimated by Equation 10 were as follows:

Pt(h k l)	(1 1 1)	(1 0 0)	(1 1 0)
b/mV	88	64	80
α	0.67	0.92	0.74

The linear relations with a slope corresponding to $\alpha \leq 1.0$ shows that the single electron transfer is the rate-determining step in all cases studied.

It is now possible to estimate Δf from Equation 8 or 11. The results are described later.

Table 1. Observed i_p, Q_0 and θ_p and calculated Δf from the i_p analysis and from wave simulation at Pt(1 1 1), (1 0 0) and (1 1 0)

	Sweep rate mV s^{-1}	i_p mA cm^{-2}	Q_0 mC cm^{-2}	θ_p	Δf (from i_p)	Δf (simulation)	k mA cm^{-2}
Pt(1 1 1)	20	0.23	0.33	0.42	0.0	−0.6	3.7×10^{-9}
	40	0.43	0.34	0.43	−0.3	−0.2	4.7×10^{-9}
	100	0.86	0.39	0.44	−1.0	−0.9	2.5×10^{-9}
	200	1.27	0.38	0.47	−1.9	−1.5	1.9×10^{-9}
Pt(1 0 0)	10	0.068	0.26	0.52	−1.7	−2.0	3.3×10^{-13}
	20	0.13	0.27	0.57	−2.2	−2.3	2.8×10^{-13}
	50	0.25	0.29	0.55	−2.7	−2.6	2.0×10^{-13}
	100	0.45	0.29	0.55	−3.0	−2.8	1.6×10^{-13}
	200	0.72	0.30	0.52	−3.4	−3.4	9.9×10^{-14}
Pt(1 1 0)	10	0.036	0.22	0.56	−3.0	−3.1	1.2×10^{-10}
	20	0.070	0.22	0.57	−3.1	−3.6	9.2×10^{-11}
	100	0.28	0.22	0.54	−3.5	−3.6	8.2×10^{-11}
	200	0.47	0.22	0.55	−4.2	−4.6	5.0×10^{-11}

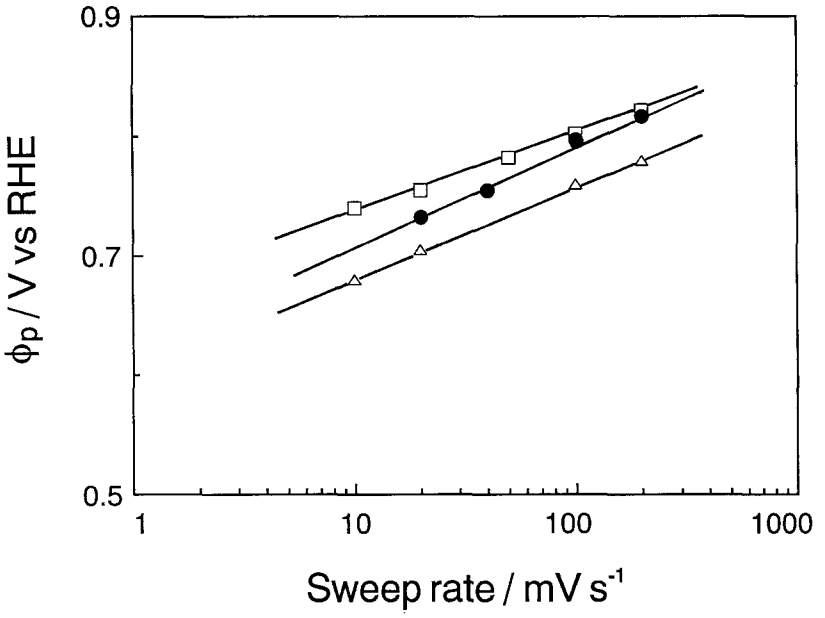

Fig. 3. Peak potential against log v (sweep rate) at 50 mV CO(a) oxidation on (○) Pt(1 1 1), (□) Pt(1 0 0) and (△) Pt(1 1 0) electrodes in phosphate buffer solution of pH 3.

4.2. *Applicability of Schemes 1 and 2*

In the case of the reversible wave of a single electron transfer step satisfying the Frumkin isotherm, the wave current is given by [2–5] (see Appendix)

$$i = -\frac{Q_0 F v}{RT}\frac{\theta(1-\theta)}{1+f\theta(1-\theta)} \qquad (13)$$

Equation 13 gives a bell shaped curve of i against θ and consequently against ϕ.

In the present case, Equations 3 and 4 were examined to ascertain whether they can reproduce the experimental oxidation waves. The relationship between θ and time is first needed.

Equations 3, 4 and 6 give the following relations:

Scheme 1: $$-\frac{1}{\theta}\exp(\Delta f\theta)\mathrm{d}\theta = \frac{k}{Q_0}\exp\left(\frac{\alpha F v}{RT}t\right)\mathrm{d}t$$

Scheme 2: $$-\frac{1}{\theta(1-\theta)}\exp(\Delta f\theta)\,\mathrm{d}\theta = \frac{k}{Q_0}\exp\left(\frac{\alpha F v}{RT}t\right)\mathrm{d}t$$

of which integration yields the relation between θ and t. In the calculation, the value of α in the above section (Fig. 2) was used and k was determined so that Equations 3 and 4 reproduce the current at a chosen potential. The θ at the chosen potential was obtained from the analysis of the peak area and Δf was taken as a parameter.

Introduction of the $\theta - t$ relation to Equations 3 and 4 gives the relation between i and t.

Figure 4(a) exemplifies calculated results of Scheme 1 where solid circles represent the experimental data on Pt(1 1 1) (Fig. 1(a), sweep rate 40 mV s^{-1}). In the calculation, $i = 0.1$ mA cm^{-2} and $\theta = 0.95$ at 0.730 V was chosen as the starting point (open circle). Equation 3 gives a peak, but its appearance differs depending on the value of Δf. ϕ_p was reproduced with $\Delta f = -6.7$ but i_p became much larger than the observed value. The peak became sharper. The value of i_p was, however, reproduced at $\Delta f = -4.0$ but instead ϕ_p become more positive than the observed

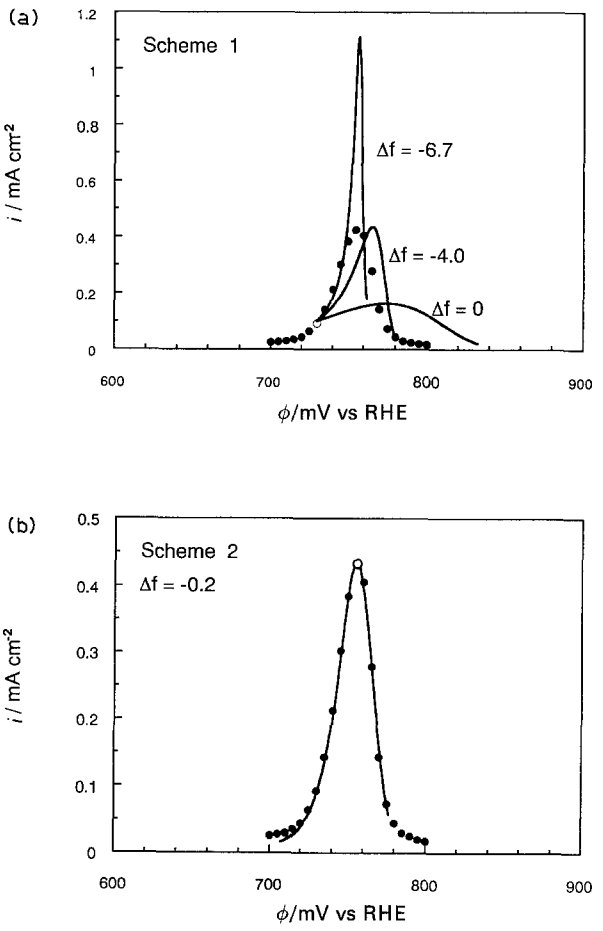

Fig. 4. Calculated oxidation wave based on (a) Scheme 1 and (b) Scheme 2. Circles represent the experimental data on Pt(1 1 1) at $v = 40$ mV s^{-1}. The open circle was taken as a starting point of the calculation. The interaction term, Δf, was taken as a parameter.

value. In addition, in the case of the calculated results, asymmetry of the peak, with a stronger tailing on the left hand side (front), is more enhanced. Consequently, it is concluded that the Scheme 1 cannot reproduce the experimental wave satisfactorily. The case of $\Delta f = 0$, was tentatively examined. The peak became less sharp as shown in Fig. 4(a).

Figure 4(b) represents the calculated result with $\Delta f = -0.2$ for Scheme 2 where the solid circles again represent the experimental data on Pt(1 1 1). In the calculation, $i_p = 0.42\,\text{mA cm}^{-2}$ and $\theta_p = 0.43$ at the peak potential, $\phi_p = 0.75\,\text{V}$, was chosen as the starting point since i_p and θ_p are estimated most accurately. The integration was extended over both sides of ϕ_p. Comparison with the experimental data (solid circles) shows a satisfactory agreement, except in the front and rear tail regions of the peak. The symmetry of the wave was much improved. It is, therefore, concluded that the oxidation of CO(a) proceeds via the pair mechanism (Scheme 2) as proposed by Gilman [17].

4.3. *Oxidation wave simulation based on Scheme 2*

The simulation was conducted for all the cases of Pt(1 1 1), Pt(1 0 0) and Pt(1 1 0) observed with different sweep rates. The starting point was set at i_p in each case. The values of i_p, ϕ_p and θ_p are listed in Table 1.

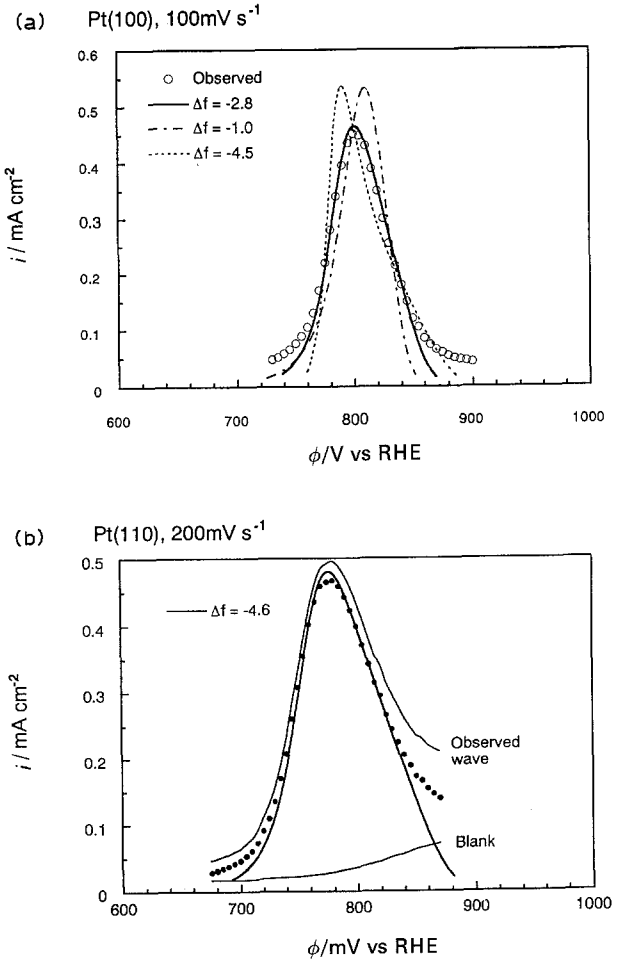

Fig. 5. Simulation of the oxidation wave of 50 mV CO(a) observed at (a) Pt(1 0 0), $v = 100\,\text{mV s}^{-1}$, and (b) Pt(1 1 0), $v = 200\,\text{mV s}^{-1}$. In Fig. 5(a), all open circles represent the observed data and in Fig. 5(b), all circles are obtained by the subtraction of the blank current.

Figure 5(a) illustrates the results calculated at Pt(1 0 0) and $100\,\text{mV s}^{-1}$. The experimental results (solid circles) were well reproduced with the value of $\Delta f = -2.8$, except the tailing parts at both sides. These deviations reflect the presence of other types of, or irregulary adsorbed, CO. Nevertheless, the latter population is very low. The Figure also shows that its larger absolute values of Δf produces a stronger rear tail with a shift of the peak in the negative direction and a smaller absolute value gives an opposite effect. This effect is in agreement with that obtained by Scheme 1, Fig. 4(a).

Figure 5(b) represents the results at Pt(1 1 0) and $200\,\text{mV s}^{-1}$. As stated earlier, the rear tail of the wave overlaps the current of the oxygen region. Subtraction of the blank oxygen region current gives the solid circles. The best fit with the solid circles was obtained at $\Delta f = -4.6$.

All Δf values thus determined on the respective planes are listed in Table 1.

4.4. *Mutual interaction in reaction atmosphere*

The comparison of the Δf values listed in Table 1 leads to the following points.

4.4.1. Validity of Δf: The two methods determining Δf from i_p analysis and the wave simulation give the same results within the accuracy of the calculation. Thus, the present Δf values will be taken to reflect the intrinsic nature of Δf.

4.4.2. Sweep-rate dependent Δf: It is interesting to note that Δf is sweep-rate dependent. The change in the interaction energy during the event that the activated complex forms from the reactants becomes larger with increase in the sweep rate. This suggests that the event occurs at a less ordered reaction environment with increase in the sweep rate. The event inevitably induces greater or lesser disordering in the near environment and takes a time for the environment to reorder at the new situation caused by the event.

4.4.3. Negative Δf: The value of Δf appears negative in all cases. The negative value may be understood in the following three ways.

Case 1: $f(\ddagger)$ and $f(\text{R})$ are repulsive (> 0) and $f(\ddagger)$ is smaller than $f(\text{R})$. The activated complex may locate more packed or further apart from the surface than the reactants and hence the repulsive interaction from the nearest adsorbates will reduce.

Case 2: $f(\ddagger)$ and $f(\text{R})$ are attractive (< 0) and the activated complex suffers from a stronger attractive interaction than the reactants, $f(\ddagger) < f(\text{R})$. Attractive interaction has been reported among adsorbed hydrogen [18, 19] (also, see Appendix). The stronger

attractive interaction may be understood when the charge transfer of the oxidation step, Equation 2, is taken into account. Because of the electron transfer, the activated complex is more or less polarized and receives a stronger attractive interaction from the nearest water molecules at the surface than the reactants do.

Case 3: The reactants receive a repulsive interaction from the nearest adsorbed species ($f(\mathrm{R}) > 0$) and the activated complex receives an attractive interaction mainly from the nearest water molecules at the surface ($f(\ddagger) < 0$).

At present, it is hard to decide which case is most plausible. Further studies will be required.

4.5. *Deviation of the simulated curve at both tailing parts*

In the above analysis, a constant Δf during the CO(a) oxidation at a given sweep rate was assumed. It is, however, possible that the Δf value changes with the CO(a) coverage. In other words, the interaction energy changes with a higher or lower order than unity with respect to the coverage. The rate expressions, Equations 3 and 4, have been deduced provided that the mutual interaction energy is linear with the coverage of the surrounding adsorbates (see Appendix, Equation 16). Figure 6 shows the value of Δf estimated from Equation 4 so that the observed current is reproduced all over the wave, where k and α were set at the values of Table 1 and Fig. 3 and θ's at the respective potentials were determined graphically. The Δf value deviates at both tailing parts of the wave. It becomes smaller at coverage close to unity and much larger at small coverages. In the intermediate region it appears almost constant, demonstrating the validity of the present analysis in the intermediate region.

In the present analysis, only one type of adsorbed CO is assumed. The *in situ IR* measurements on Pt(1 1 1), (1 0 0) and (1 1 0) show a predominant presence of the linear CO [20] and a small amount of the bridged CO [21] in acidic solutions at full coverage, respectively. The deviations may be partly attributed to the adsorbed species present to a minor extent.

Appendix: Analysis of the reversible voltammogram

The hydrogen ion discharge reaction at a platinum electrode,

$$\mathrm{H^+ + e^- \rightleftharpoons H(a)} \tag{14}$$

is a typical example which gives a reversible voltammogram, where H(a) denotes the adsorbed hydrogen atom.

The equilibrium condition of Equation 14 gives the following relation [6, 7]

$$\exp\left(-\frac{\mu_{\mathrm{H^+}} + \mu_{\mathrm{e^-}}}{RT}\right) = \frac{1-\theta}{\theta}\exp\left(-\frac{\epsilon_{\mathrm{H}}}{RT}\right) \tag{15}$$

where $\mu_{\mathrm{H^+}}$ and $\mu_{\mathrm{e^-}}$ are the electrochemical potentials of $\mathrm{H^+}$ and $\mathrm{e^-}$, θ the coverage and ϵ_{H} the potential energy of the adsorbed hydrogen, respectively. It is assumed that interaction energy varies linear with the coverage, i.e.

$$\epsilon_{\mathrm{H}} = \epsilon_{\mathrm{H},0} + f'\theta \tag{16}$$

where f' is the interaction energy at $\theta = 1$. Since $\mu_{\mathrm{e^-}}$ is expressed as the sum of the chemical part $\mu_{\mathrm{e^-},0}$ and the electrical part $-F\phi$ (ϕ, the electrode potential), one obtains

$$\frac{\theta}{(1-\theta)} = K\exp(f\theta)\exp\left(\frac{F\phi}{RT}\right) \tag{17}$$

where

$$f \equiv \frac{f'}{RT} \quad \text{and} \quad K \equiv \exp\left(-\frac{\epsilon_{\mathrm{H},0} + \mu_{\mathrm{H^+}} + \mu_{\mathrm{e^-},0}}{RT}\right)$$

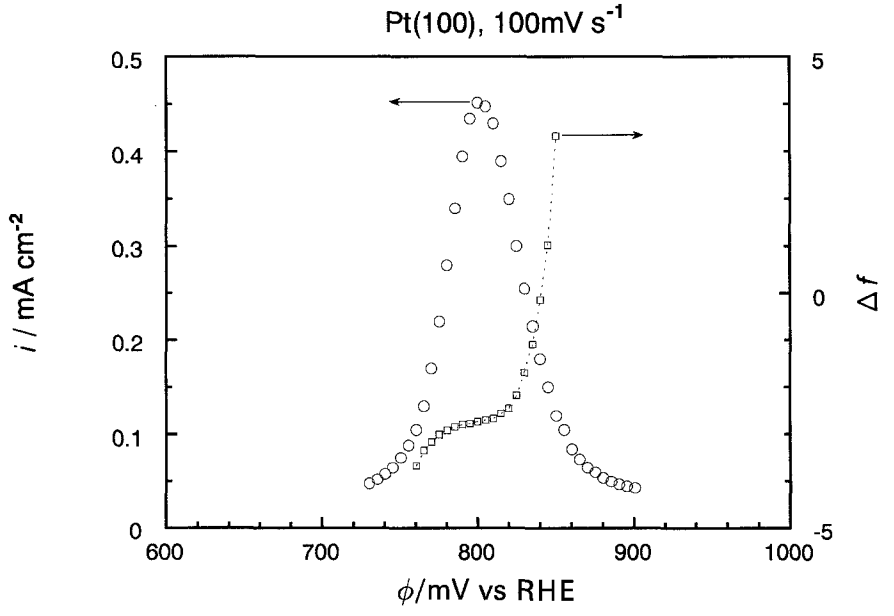

Fig. 6. Estimation of Δf (□) on Pt(1 0 0) by Equation 4 using i, θ at respective potentials and k determined at the peak potential. Circles represent the observed data.

A positive f means repulsive and a negative f means attractive interaction, respectively.

Based on the above isotherm, voltammograms are obtained as follows. The current of the anodic wave of the voltammogram, $i/\mathrm{mA\,cm^{-2}}$, is given as

$$i = -Q_0 \frac{d\theta}{dt} = -Q_0 v \frac{d\theta}{d\phi} \tag{18}$$

where $Q_0/\mathrm{mC\,cm^{-2}}$ is the monolayer charge of the adsorbed hydrogen and $v/\mathrm{mV\,s^{-1}}$ is the sweep rate. Equations 17 and 18 yield Equation 13 in the text. Equation 13 shows that i is proportional to v and becomes zero at $\theta = 0$ and 1, respectively. The peak current, $i_p/\mathrm{mA\,cm^{-2}}$, is obtained by the condition of the derivative of Equation 13 being equal zero, as Equation 7 in the text. i_p is $Q_0 Fv/RT$ for the Langmuir case, being $0.20\,\mathrm{mA\,cm^{-2}}$ at $v = 100\,\mathrm{mV\,s^{-1}}$, $Q_0 = 0.21\,\mathrm{mC\,cm^{-2}}$ and 25°C. i_p becomes larger (smaller) with an attractive (repulsive) interaction than that of the Langmuir's and becomes infinite at $f = -4.0$ [4]. Equation 7 is useful to assess the nature of interaction, as well as to estimate its value. Separate experiment at Pt(1 1 0) in 0.5 M H_2SO_4 gives $i_p = 0.28\,\mathrm{mA\,cm^{-2}}$ at $100\,\mathrm{mV\,s^{-1}}$. Equation 7 with $Q_0 = 0.15\,\mathrm{mC\,cm^{-2}}$ gives $f = -1.9$. The negative value represents the attractive interaction among the adsorbed hydrogen.

The width at a half height of the wave is obtained from the condition that $i/i_p = 1/2$ which gives

$$\theta = \frac{1}{2}\left\{1 \pm \left(\frac{4+f}{8+f}\right)^{1/2}\right\}$$

The corresponding potentials to the above θ's are given from Equation 17 and the difference between them gives the width at half height, $\Delta\phi_{1/2}$ [22, 23], i.e.

$$\Delta\phi_{1/2} = \frac{2RT}{F} \ln \frac{1+g}{1-g} + \frac{RT}{F} fg \tag{19}$$

where

$$g \equiv \left[\frac{(4+f)}{8+f}\right]^{1/2}$$

Equation 19 shows that $\Delta\phi_{1/2}$ is independent of v, Q_0 and θ, being 90 mV at 25°C for $f = 0$ and becomes smaller (larger) with an attractive (repulsive) interaction than that of the Langmuir's, being zero at $f = -4.0$. This relation is also useful in assessing the nature of interaction as well as to estimate its extent. The $\Delta\phi_{1/2}$ of the hydrogen wave at Pt(1 1 0) was observed as 43 mV in 0.5 M H_2SO_4 and f is estimated as -1.8, which is in agreement with the above value of -1.9.

References

[1] J. O'M. Bockris and H. Kita, *J. Electrochem. Soc.* **108** (1961) 676.
[2] B. E. Conway and E. Gileadi, *Trans. Faraday. Soc.* **58** (1962) 2493.
[3] S. Srinivasan and E. Gileadi, *Electrochim. Acta* **11** (1966) 321.
[4] H. Angerstein-Kozlowska, J. Klinger and B. E. Conway, *J. Electroanal. Chem.* **75** (1977) 45.
[5] E. Gileadi and B. E. Conway, 'Modern Aspects of Electrochemistry', (edited by J. O'M. Bockris and B. E. Conway), Vol. 3, Butterworth, London (1964) Chapter 5.
[6] H. Kita, *J. Res. Inst. Catalysis, Hokkaido Univ.* **17** (1969) 79.
[7] J. Horiuti and H. Kita, *ibid.* **12** (1964) 122.
[8] H. Matsuda, K. Aoki and K. Tokuda, *J. Electroanal. Chem.* **217** (1987) 1.
[9] H. Matsuda, K. Aoki and K. Tokuda, *ibid.* **217** (1987) 15.
[10] B. Beden, C. Lamy, N. R. Tacconi and A. J. Arvia, *Electrochim. Acta* **35** (1990) 691.
[11] J. M. Leger, B. Beden, C. Lamy and S. Bilmes, *J. Electroanal. Chem.* **170** (1984) 305.
[12] J. Clavilier, R. Faure, G. Guinet and R. Durand, *ibid.* **107** (1980) 205.
[13] H. Kita, S. Ye, A. Aramata and N. Furuya, *ibid.* **295** (1990) 317.
[14] H. Kita, K. Shimazu and K. Kunimatsu, *ibid.* **248** (1988) 163.
[15] C. Gutiérrez and J. A. Caram, *ibid.* **308** (1991) 321.
[16] H. Kita, S. Ye and K. Sugimura, *ibid.* **297** (1991) 283.
[17] S. Gilman, *J. Phys. Chem.* **66** (1962) 2657; **67** (1963) 78; **67** (1963) 1898; **68** (1964) 70.
[18] B. Love, K. Seto and J. Lipkowski, *J. Electroanal. Chem.* **199** (1986) 219.
[19] D. Armand and J. Clavilier, *ibid.* **225** (1987) 205; **233** (1987) 251.
[20] N. Furuya, S. Motoo and K. Kunimatsu, *ibid.* **239** (1988) 347.
[21] S. Chang and M. J. Weaver, *Surf. Sci.* **238** (1990) 142.
[22] E. Laviron, *J. Electroanal. Chem.* **52** (1974) 395.
[23] A. Sadkowski, *ibid.* **97** (1979) 283.